JOURNAL OF ENVIRONMENTAL SCIENCES 150 (2025) 582–593

Available online at www.sciencedirect.com

ScienceDirect

www.elsevier.com/locate/jes

JES JOURNAL OF ENVIRONMENTAL SCIENCES

www.jesc.ac.cn

Research Article

Cd/Pb behavior during combustion in a coal-fired power plant and their spatiotemporal impacts on soils: New insights from Cd/Pb isotopes

Yafei Xia[1,2,3], *Ting Gao*[1], *Yuhui Liu*[1], *Meng Qi*[1,3], *Jian-Ming Zhu*[4], *Hui Tong*[2], *Yiwen Lv*[2], *Chengshuai Liu*[1,2,*]

[1] *State Key Laboratory of Environmental Geochemistry, Institute of Geochemistry, Chinese Academy of Sciences, Guiyang 550081, China*

[2] *National-Regional Joint Engineering Research Center for Soil Pollution Control and Remediation in South China, Guangdong Key Laboratory of Integrated Agro-environmental Pollution Control and Management, Guangdong Institute of Eco-environmental Science & Technology, Guangdong Academy of Sciences, Guangzhou 510650, China*

[3] *University of Chinese Academy of Sciences, Beijing 100049, China*

[4] *State Key Laboratory of Geological Processes and Mineral Resources, China University of Geosciences, Beijing 100083, China*

ARTICLE INFO

Article history:
Received 14 December 2023
Revised 2 March 2024
Accepted 3 March 2024
Available online 16 March 2024

Keywords:
Heavy metal diffusion
Coal combustion
Source tracing
Atmospheric deposition
Isotope fractionation
Soil pollution

ABSTRACT

Coal power plants annually generate quantities of byproducts that release environmentally hazardous heavy metals like Cd and Pb. Understanding the behavior and spatiotemporal impacts on soils of these releases is crucial for pollution control. This study investigated the concentrations and isotope ratios of Cd/Pb in combustion byproducts, depositions and soils collected from a coal-fired power plant or its surrounding area. The pulverized fuel ash (PFA) and desulfurized gypsum (DG) exhibited heavier Cd isotopes with Δ^{114}Cd values of 0.304‰ and 0.269‰, respectively, while bottom ash (BA) showed lighter Cd isotopes ($\Delta^{114}Cd_{BA\text{-}coal} = -0.078$‰), compared to feed coal. We proposed a two-stage condensation process that governs the distribution of Cd/Pb, including accumulation on PFA and DG within electrostatic precipitators and desulfurization unit, as well as condensation onto fine particles upon release from the stack. Emissions from combustion and large-scale transport make a significant contribution to deposition, while the dispersion of Cd/Pb in deposition is primarily influenced by the prevailing wind patterns. However, the distribution of Cd/Pb in soils not only exhibit predominant wind control but is also potentially influenced by the resuspension of long-term storage byproducts. The power plant significantly contributes to soil in the NW–N–NE directions, even at a considerable distance (66%–79%), demonstrating its pervasive im-

* Corresponding author.
E-mail: liuchengshuai@vip.gyig.ac.cn (C. Liu).

https://doi.org/10.1016/j.jes.2024.03.002

pact on remote regions along these orientations. Additionally, based on the vertical behavior in the profile, we have identified that Cd tends to migrate downward through leaching, while variations in Pb respond to the historical progression of dust removal.

Introduction

Coal-fired power generation remains the predominant source of electricity globally and plays a pivotal role in the socioeconomic advancement of nations (Habib and Khan, 2021). Coal combustion usually generates various byproducts with large amounts of heavy metals, including combustion bottom ash (BA), pulverized fuel ash (PFA) captured by electrostatic precipitators, flue gas (FG) escaping into the atmosphere, and desulfurized gypsum (DG) (Li et al., 2018; Park et al., 2018). The dispersion of these wastes into the surrounding soils poses a potential threat to human health through the food chain, thereby giving rise to persistent concerns regarding the dissemination of heavy metals resulting from coal combustion (Raj and Maiti, 2020; Tong et al., 2023a). However, to date, limited information is available regarding the behavior and influencing factors of Cd and Pb among these byproducts during coal combustion within power plants.

Previous studies have demonstrated that the fine-grained fraction of these products exhibits higher concentrations of heavy metals, such as Cd and Pb, compared to the coarse-grained fraction (Kotelnikova et al., 2022; Tong et al., 2023b). During high-temperature coal combustion (typically approximately 1500°C), a significant portion of Cd and Pb tends to volatilize and subsequently condense onto fine particles due to their larger surface area (Meij and Winkel, 2007). Despite electrostatic precipitators exhibiting a high retention rate for large particles (~99%), their efficiency significantly decreases for particles smaller than 0.8 μm that remain in the flue gas (Nussbaumer, 2007). These particles, emitted from flue gas pipes, disperse through wind-induced diffusion and play a significant role in transporting Cd and Pb into the surrounding soils. However, tracing these fine atmospheric deposit fines in soil near coal-fired power plants presents greater challenges compared to large-scale acute coal ash spills such as BA and PFA.

Several studies have found that the spatial distribution of Cd and Pb in soils around coal-fired power plants is not always related to prevailing wind (da Silva Júnior et al., 2019; Linnik et al., 2019; Tsikritzis et al., 2002). This suggests that other factors jointly control Cd and Pb accumulation in soils around coal-fired power plants. In addition to the fine-grained fraction of combustion byproducts, the captured byproducts (such as PFA, BA, and DG) are often stored in open areas and concentrated in landfills or used for secondary purposes (Li et al., 2018). These processes pose a potential risk of heavy metal re-release into the surrounding soil, thereby contributing to a diverse source of Cd and Pb in deposition and soil (Park et al., 2018). The emissions of heavy metals from power plants are influenced by factors such as energy consumption capacity and the efficiency of particulate matter removal, exhibiting distinct temporal variations that contribute to diverse cumulative impacts on soil (Schneider et al., 2014). Additionally, historically deposited heavy metals may suffer from post-depositional processes in soils, such as leaching (Schneider et al., 2021). This may result in vertical redistribution of previously deposited Cd and Pb within topsoils, consequently altering their spatial distribution driven by factors like wind patterns (Mandal and Sengupta, 2006). Despite some attention given to the distribution of heavy metals in soil surrounding power plants (Tanić et al., 2018; Tong et al., 2023b; Vardar et al., 2022; Wang and Zhang, 2021), limited research has been conducted on the factors governing the spatiotemporal distribution of Cd and Pb in soils. This knowledge gap hinders effective management strategies for addressing pollution risks associated with Cd and Pb contamination in soils around coal-fired power plants. A comprehensive understanding of the dispersion and fate of Cd and Pb around power plants can be achieved by developing a spatial cognition framework that considers both point-plane relationships, along with a temporal cognition framework that incorporates contemporary observations with historical activities.

Stable isotopes have proven to be a robust tool for tracing the origin and migration of heavy metals in environmental systems (Wang et al., 2021a; Wiederhold, 2015). For example, the absence of fractionation in Pb isotopes during industrial and environmental processes (Bi et al., 2017) provides accurate information about the initial sources and pathways of heavy metals. However, limited Pb isotope fractionation during coal combustion may lead to a consistent Pb isotope ratio of different combustion byproducts (Wang et al., 2023). Consequently, it is difficult to distinguish their contributions in soils solely based on Pb isotopes. In contrast, previous studies have confirmed that high-temperature processes, such as smelting (Chrastný et al., 2015), induce significant isotopic fractionation of Cd, with lighter Cd isotopes preferentially entering the gas phase while heavier isotopes become enriched in residual materials. This characteristic offers an opportunity to utilize Cd isotopes as a valuable tool for discerning the input of diverse combustion byproducts in atmospheric deposition or soils (Zhong et al., 2020). Additionally, based on the Cd isotope fractionation characteristics during various biogeochemical processes (e.g., leaching and adsorption) (Xie et al., 2021; Yan et al., 2021a), further investigation into the subsequent fate of Cd following its sedimentation into soils could be pursued. Therefore, the integration of Pb and Cd isotopes may provide new insights into the diffusion and fate of Cd and Pb in soils surrounding coal-fired power plants.

The aim of this study is to investigate Cd and Pb behavior during combustion, assess their spatial distribution as well as short- and long-term variability in soils surrounding a coal-fired power plant, and explore potential associations with pollution sources. To this end, we conducted concentrations and isotopic analyses on the combustion byproducts, surrounding

top soils, and depositions. We examined the behavior of Cd and Pb during high-temperature coal combustion and subsequently comprehensively assessed their dispersion patterns in various directions, while simultaneously monitoring their impact on soil accumulation at different distances. Finally, we investigated variations in Cd and Pb isotope characteristics within a soil profile in response to post-depositional or historically deposited processes. The findings of this study are expected to enhance the comprehension of heavy metal behavior in coal-fired power plants and their impact on the surrounding environment, ultimately guiding improved strategies for controlling pollution.

1. Materials and methods

1.1. Study area

This study was undertaken within areas of a coal-fired power plant in Guangdong Province, South China (113°35′2″E, 24°35′17″N; Fig. 1), situated approximately 39 km south of Shaoguan City. Since 1967, when the inaugural 50,000 kilowatt unit was commissioned, this power plant has emerged as a prominent facility within the Guangdong power system. With an average daily coal consumption of approximately 2000 tons, it serves as one of the primary sources of electricity supply in South China (Wang et al., 2016). This region is characterized by a humid monsoon climate, predominantly influenced by the year-round monsoon and the Nanling Mountains, resulting in a complex and diverse mid-subtropical climate regime. The prevailing wind directions in this region include N, NNW, S, and, SSW (Appendix A Fig. S1, averaged between 2000 and 2019; all data were collected from the China Meteorological Administration, http://data.cma.cn/). The parent rock of soils primarily comprises silicate rock, while the soil types are characterized as latosolic soil.

1.2. Sample collection and preparation

The sampling sites were arranged from eight different directions centered around the coal-fired power plant (Fig. 1). The sampling sites from south (S1, S2, S3), west (W1, W2, W3), north (N1, N2, N3), northeast (NE1, NE2, NE3), northwest (NW1, NW2, NW3), and southeast (SE1, SE2, SE3) are located at distances of 0.5 km, 1 km, and 2 km from the power plant, respectively. The sampling sites from the southwest (SW2, SW3) are 1 km and 2 km, and those from the east (E1, E3) are 0.5 km and 2 km distant from the power plant. The inconsistency of distances is caused by the cutoff of the Beijiang River and mountains (Fig. 1). Given the similarity between the prevailing wind directions during the 20-year averaged March period and annual prevailing wind directions (Appendix A Fig. S1), we specifically collected dry depositions in March 2021. A total of 22 dry deposition samples were collected on a precleaned cellulose filter (No. 41, Whatman PLC, UK) using a manually deployed bracket (2 m above ground level) with a settling cylinder (Anshun experimental supplies factory, China). After 96 hours of settling, the filters with deposition samples were sealed in airtight plastic bags (Franssens et al., 2004). The filter is weighed before and after settlement collection to determine the total mass of the deposited material.

A total of 22 top soil samples were also collected at the same sampling sites, with each sample comprised 4–6 subsamples (0–10 cm) obtained in a checkerboard pattern surrounding each site. Top soil samples were sealed in airtight plastic bags and then transported to the laboratory. A soil profile was sampled from a location downwind of the coal-fired power plant (site #NE2), and a total of six soil samples were collected along the profile based on the depth, soil color variations, and soil texture characteristics. In the lab, each soil sample was dried at room temperature until it reached a constant weight. Subsequently, a meticulous manual removal of all plant residues and gravel was conducted, followed by thor-

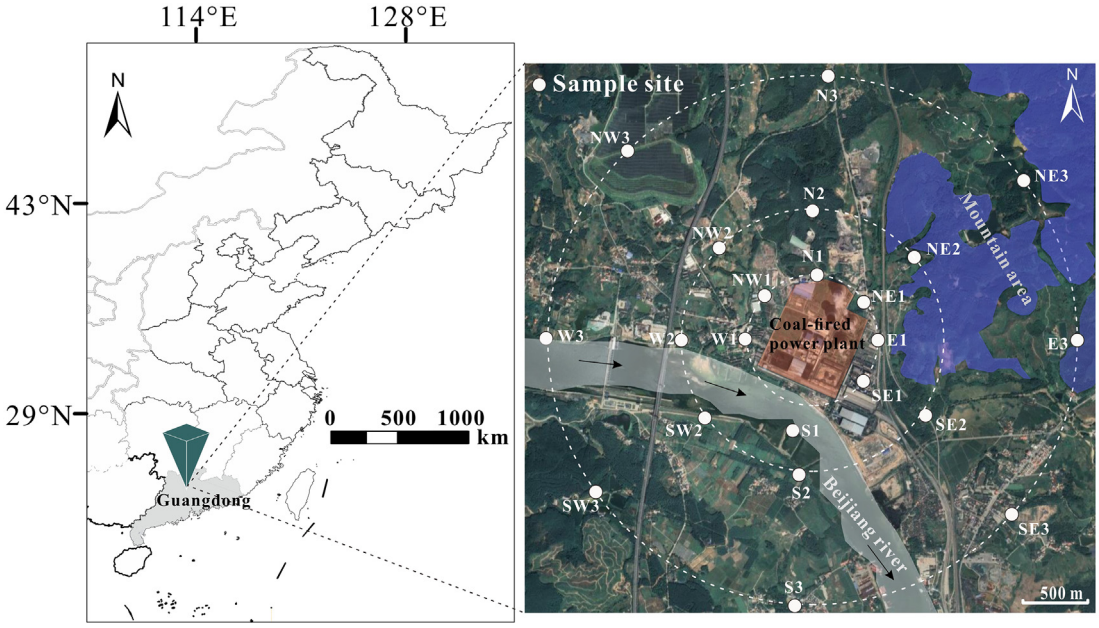

Fig. 1 – Map of the study coal-fired power plant and location of the sampling sites.

ough soil mixing through a 2-mm mesh sieve. The sample was then ground using a ceramic mortar until it passed through a 200-mesh sieve.

Additionally, coal-fired combustion products, including feed coal (FC), BA, PFA, and DG, were collected from the power plant (Appendix A Fig. S2). Particulate matter fraction ($PM_{2.5}$, PM_{10}, and TSP) samples were collected in close proximity to the plant using an air sampler (Changshu Mine Mechanical and Electrical Equipment Co. Ltd., China) at a flow rate of 100 L/min onto a precleaned Whatman® 41 cellulose filter (Whatman PLC, UK).

1.3. *Laboratory analysis*

1.3.1. *Sample digestion*

HNO_3, HCl, and HF (BV-III, Beijing Institute of Chemical Reagents, China) used during sample treatments were further distilled by subboiling distillation (DST-1000, Savillex, USA) and ultrapure water was obtained from a Milli-Q system (Milli-Q Advantage A10, Merck Millipore, USA). Approximately 50–100 mg soil and combustion product samples were transferred into Teflon breakers (Savillex, UAS) and digested using a 4 mL mixture of HF-HNO_3 (1:3, *V/V*) at 140°C for 48 hr. After the solutions were dried at 160°C and then refluxed and evaporated twice in 0.3 mL of HNO_3 to remove the excess fluorides, 3.2 mL of aqua regia was added to the dried samples and heated at 120°C, and the residual samples were digested until complete dissolution. The cellulose filters with deposition samples were cut into pieces and digested with 7 mL of HNO_3 and 3 mL of HF using a microwave digestion system (Ethos UP, Milestone, Italy). The solutions were transferred to Savillex® Teflon breakers and dried at 160°C for subsequent aqua regia digestion with the same procedure used for solid samples. Finally, each sample solution was dissolved in 10% HNO_3 (*m/m*) for subsequent analysis.

1.3.2. *Cd and Pb concentrations*

Cd and Pb concentrations were determined by graphite furnace atomic absorption spectroscopy (AAS, PinAAcle 900Z, PerkinElmer, USA). The minimum detection limits (in μg/g) in the studied samples are 0.01 for Cd and 0.1 for Pb. The analytical precision and accuracy were determined by analyzing the Chinese National Standard soil reference sample (GSS-1, 4.66 μg/g for Cd, 102 μg/g for Pb), and the results showed good agreement with the recommended values (Appendix A Table S1). The concentrations of Cd and Pb in the blank sample are below the detection limit of the instrument. The relative standard deviations (RSDs) of our measurements were better than 10%.

1.3.3. *Cd and Pb purification for isotope analyses*

All reagents (HNO_3, HCl, and HF (Beijing Institute of Chemical Reagents, China); HBr (Aladdin, China); H_2O_2 (Fisher Scientific, USA)) were ultrapure grade and prepared with ultrapure water from a Milli-Q system (Milli-Q Advantage A10, Merck Millipore, USA). Purification of Cd was conducted at the Isotope Geochemistry Laboratory of China University of Geosciences (Beijing). The stable Cd isotope compositions were determined using a double spike technique through measurement on a multiple collector inductively coupled plasma mass spectrometer (MC–ICP–MS, Neptune Plus, Thermo Scientific, USA). The purification procedure has been reported in Tan et al. (2020). Briefly, digested samples mixed with a ^{111}Cd-^{113}Cd double spike were loaded onto a column filled with 2.8 mL AG MP-1 resin (100–200 mesh, Bio-Rad, USA). Matrix elements were removed by washing first with 10 mL of 2 mol/L HCl and then with 10 mL of 1 mol/L HCl. Cd was collected in 20 mL of 0.0012 mol/L HCl after sequentially adding 20 mL of 0.3 mol/L HCl, 20 mL of 0.06 mol/L HCl, and 10 mL of 0.012 mol/L HCl to elute Pb, Zn and Sn. The dried Cd separates were dissolved in 2 mL of 2 mol/L HCl, and the same column procedure was repeated to obtain a further purified Cd solution for isotopic analyses. Cd separates were dried, followed by the addition of 3 mL HNO_3 and 1 mL 30% H_2O_2 to digest the possible organic matter. Finally, the samples were evaporated to incipient dryness on a hot plate at 80°C and redissolved in 1 mL of 2% HNO_3–0.1% HF for isotopic analysis. The certified reference materials NOD-P-1 (United States Geological Survey, USA) and GSS-1 (Institute of Geophysical Geochemistry Research of the Chinese Academy of Geological Sciences, China) were processed following the same protocol.

Pure Pb solution was separated by chromatographic columns in a class-1000 clean room equipped with class-100 laminar flow hoods at the Guangdong Institute of Eco-environmental Science & Technology, Guangzhou, China. HCl, HBr, and HF were distilled twice by subboiling distillation (DST-1000, Savillex, USA). All wares used in sample preparation were cleaned following a strict procedure. Samples containing approximately 200–500 ng of Pb were loaded onto a column filled with 0.8 mL AG1-X8 resin (100–200 mesh, Bio-Rad, USA) (Xia et al., 2023). The resin was first activated with anhydrous ethanol (Aladdin, China) and sodium hydroxide (Aladdin, China) and then cleaned alternately with Milli-Q water and 6 mol/L HCl. Matrix elements were removed by washing with 1 mol/L HBr and then with 2 mol/L HCl. Pb was collected in the following 1.5 mL of 6 mol/L HNO_3. After Pb separates were evaporated to dryness at 80°C, 0.2 mL HNO_3 and 0.6 mL HCl were added to digest the possible organic matter, followed by the addition of 0.8 mL of concentrated HNO_3 to remove HCl. Finally, the evaporated samples were redissolved in 1 mL 3% HNO_3 (*m/m*) for isotopic analysis.

1.3.4. *Cd and Pb isotope measurements*

Cd isotope compositions were determined by MC–ICP–MS at China University of Geoscience, Beijing, China. An Aridus-II desolvator (Teledyne CETAC Technologies Omaha, USA) was used to introduce the samples (Chang et al., 2023; Lu et al., 2023; Tan et al., 2020). A spiked NIST-3108 (National Institute of Standards and Technology, USA) solution was bracketed every 5 samples to correct for instrumental drift. The total procedural blanks (from sample dissolution to mass spectrometry) were routinely measured and had an average of 0.04 ng for Cd, which is considered neglected during mass spectrometry. The Cd isotope compositions were reported relative to the NIST 3108 Cd isotope reference material using a δ notation based on the $^{114}Cd/^{110}Cd$ ratio expressed as $\delta^{114}Cd$ (‰) = $[(^{114}Cd/^{110}Cd)_{sample}/(^{114}Cd/^{110}Cd)_{NIST\text{-}3108}\text{-}1] \times 1000$. The geological reference materials NOD-P-1 ($\delta^{114}Cd = 0.140‰ \pm 0.025‰$) and GSS-1 ($\delta^{114}Cd = 0.123‰ \pm 0.046‰$) were analyzed together with the samples for quality control, and the results

showed good agreement with published values (Tan et al., 2020).

The Pb isotopic ratios of all samples were measured on a Neptune Plus MC–ICP–MS (Thermo Scientific, USA) at the Institute of Geochemistry, Chinese Academy of Sciences, China. The total Pb procedure blank for the whole analyses is less than 0.008 ng per analysis. The NIST 981 (National Institute of Standards and Technology, USA) solution was diluted to 50 ppb in 3% HNO_3 (*m*/*m*) with 10 ppb of thallium (Tl, NIST 997, National Institute of Standards and Technology, USA) added as an internal standard for mass fractionation correction ($^{205}Tl/^{203}Tl$=2.3871). The obtained values of NIST 981 were 2.1666 ± 0.0018 and 0.9146 ± 0.00009 for $^{208}Pb/^{206}Pb$ and $^{207}Pb/^{206}Pb$, respectively, and were similar to other internationally cited references (He et al., 2019; Zhao et al., 2015).

1.3.5. *Data analysis*

The sedimentation fluxes of Cd and Pb at each sampling point were calculated by Eqs. (1)-(2) (Marticorena et al., 2017):

$$F_i = (M_D \times C_i)/S \times t \quad (1)$$

$$S = 2 \times 3.14 \times \frac{d^2}{4} \quad (2)$$

where, F_i (μg/(m^2·hr)) and C_i (μg/g) are the sedimentation flux and mass fraction of element *i* (Cd or Pb); M_D (g) is the mass of deposition (data presented in Appendix A Table S1); *d* (cm) is the inner diameter of the sampler, which is 16 cm in this study, each sampling point is placed with two sampling buckets; *S* (m^2) is the collection area of each sampling point and can be calculated to be 0.0402 m^2; *t* (hr) is the settling time.

The magnitude of the fractionation ($\Delta^{114}Cd_{A\text{-}B}$) can be estimated by comparing the isotopic composition of A and B ($\delta^{114}Cd_A$, $\delta^{114}Cd_B$) (Zhu et al., 2002): $\Delta^{114}Cd_{A-B} = \delta^{114}Cd_A - \delta^{114}Cd_B$.

The MixSIAR Bayesian isotope mixing model was used to calculate the relative contributions of the various sources. It takes into account uncertainties in isotopic values and allows for both analytical uncertainty and source heterogeneity (Moore and Semmens, 2008). The Pb isotope compositions in the soils and end members were utilized as input parameters in MixSIAR. More details on the calculations were reported in our previous study (Xia et al., 2023).

2. Results

2.1. *Cd and Pb concentrations*

The coal-fired combustion products FC, PFA, and BA exhibited significantly different Cd concentrations, with average values of 0.07 μg/g, 1.15 μg/g, and 0.90 μg/g, respectively (Appendix A Table S1), and relatively high Pb concentrations, with average values of 15 μg/g, 97 μg/g, and 56 μg/g, respectively. The concentrations of Cd and Pb in DG (1.27 μg/g for Cd, 73 μg/g for Pb) were comparable to those found in PFA. For the top soils, Cd and Pb concentrations had similar spatial distributions, with higher concentrations in the NE–E and SW–S directions than in the other directions. Specifically, the concentrations of Cd in the top soil varied from 0.15 to 1.97 μg/g, with an average value of 0.76 ± 0.51 μg/g, and the concentrations of Pb ranged from 31 to 119 μg/g, with an average value of 70 ± 27 μg/g (Appendix A Table S1). The concentrations of Cd and Pb in the soil profile exhibited variations within the depth range of 0–90 cm (0.20 to 2.24 μg/g for Cd, 24 to 104 μg/g for Pb). The concentrations of Cd and Pb in the depositions were calculated based on the mass of total deposition collected. As shown in Appendix A Table S1, the concentrations of Cd ranged from 0.15 to 1.43 μg/g, while those of Pb ranged from 4 to 117 μg/g, with average values of 0.55 ± 0.37 μg/g and 25 ± 25 μg/g, respectively.

2.2. *Cd and Pb isotope ratios*

The Cd and Pb isotope compositions of all samples are presented in Appendix A Table S1. The FPA and DG exhibited relatively heavier Cd isotope compositions with $\delta^{114}Cd$ values of 0.621‰ ± 0.028‰ and 0.586‰ ± 0.026‰, respectively, while BA showed lighter Cd isotope composition with a $\delta^{114}Cd$ value of 0.238‰ ± 0.037‰, compared to FC (0.317‰ ± 0.037‰). The Cd isotopic compositions of $PM_{2.5}$, PM_{10}, and TSP were 0.102‰ ± 0.060‰, 0.392‰ ± 0.050‰, and 0.521‰ ± 0.045‰, respectively, showing a significant dependence on particle size. The Cd isotope compositions in atmospheric deposition varied from –0.123‰ ± 0.060‰ to 0.499‰ ± 0.001‰, and light Cd isotopes were relatively enriched in the E–SE direction compared with other directions. The Cd isotope compositions of top soils exhibited a wide variation, with $\delta^{114}Cd$ values ranging from –0.155‰ ± 0.058‰ to 0.897‰ ± 0.059‰, and light Cd isotopes were relatively enriched in the N direction compared with other directions. In the soil profile, the average Cd isotope composition of the upper horizon (0–30 cm, 0.304‰ ± 0.264‰) was heavier than that of the lower horizon (30–90 cm, –0.055‰ ± 0.213‰).

The Pb isotope ratios of FC, PFA, DG, and BA were 2.1121, 2.0831, 2.0896, and 2.0741 for $^{208}Pb/^{206}Pb$, respectively. The deposition samples exhibited $^{208}Pb/^{206}Pb$ ratios ranging from 2.0095 to 2.1161, with an average of 2.1069 ± 0.0032. The Pb isotope ratios of the top soils varied greatly from 2.0618 to 2.1017 for $^{208}Pb/^{206}Pb$. The topmost layer of the soil profile exhibited a higher $^{208}Pb/^{206}Pb$ value of 2.0978, while the remaining layers showed minimal variation in $^{208}Pb/^{206}Pb$ with an average value of 2.0686 ± 0.0130.

2.3. *Cd and Pb fluxes of deposition*

The deposition fluxes of Cd and Pb are shown in Appendix A Table S1. The fluxes of Cd and Pb exhibited a disparity exceeding an order of magnitude, with Pb fluxes ranging from 3.4 μg/(m^2·hr) to 141 μg/(m^2·hr), while Cd fluxes ranging from 0.2 mg/(m^2·hr) to 3.9 mg/(m^2·hr); nevertheless, they exhibited analogous distribution patterns. The Cd and Pb fluxes in the S, N, and E directions exhibited significantly higher values than those in the other directions. Specifically, the highest fluxes of Cd and Pb were observed in the S direction at site #S1 for Cd and site #S3 for Pb, while the lowest fluxes of these two metals were recorded at site #W3.

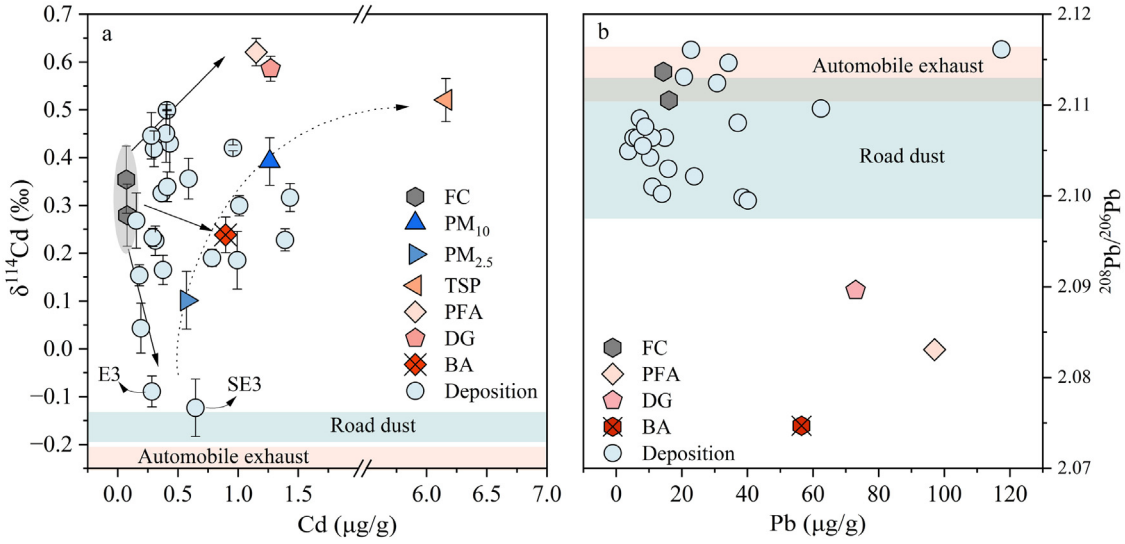

Fig. 2 – Relationship of the concentration and isotope ratios of Cd (a) and Pb (b) in deposition, coal, and byproducts. The Cd isotope compositions of road dust and automobile exhaust were obtained from Fang et al. (2022), Yan et al. (2021b), and Zhang et al. (2020), and the Pb isotope ratios were obtained from Duzgoren-Aydin (2007) and Wang et al. (2021b). FC: feed coal; $PM_{2.5}$, PM_{10}, and TSP: Particulate matter fraction; PFA: pulverized fuel ash; DG: desulfurized gypsum; BA: bottom ash.

3. Discussion

3.1. *Behavior of Cd and Pb within the power plant*

The average concentrations of Cd and Pb in FC were 0.07 μg/g and 15 μg/g, respectively, which were significantly lower than those observed in combustion residue (Fig. 2). This implies a continuous process of Cd and Pb accumulation and enrichment within waste generated at combustion facilities. It is commonly believed that lighter Cd isotopes tend to be more easily volatilized, while heavier isotopes remain in the residual during high-temperature processes, with $\Delta^{114}Cd_{solid\text{-}gas}$ values ranging from 7% to 20‰ (Chrastný et al., 2015; Cloquet et al., 2006; Fouskas et al., 2018; Zhang et al., 2020). In coal with an ash content less than 5%, Cd can be combined with organic matter and entrained into the flue ash during combustion (Meij and Winkel, 2007), potentially exhibiting preferential release of these organically bound Cd that are commonly enriched in heavy isotopes (Wiggenhauser et al., 2021; Zhao et al., 2021). Therefore, if Cd combined with combustible organic matter in coal evaporates incompletely, residual materials (i.e., BA) would greatly enrich heavy Cd isotopes. However, the BA and FC samples show relatively limited Cd isotope fractionation in this study (Fig. 2a), with a $\Delta^{114}Cd_{BA\text{-}FC}$ value of –0.079‰. Based on the principle of mass conservation, it is reasonable to postulate that the evaporated material exhibits a Cd isotopic composition near that of the FC (Zhong et al., 2020). Therefore, the underlying mechanism of Cd isotope fractionation during coal combustion involves the near-complete volatilization of Cd combined with combustible organic matter, resulting in evaporated Cd that likely demonstrates a Cd isotope composition comparable to that of the initial coal.

Following evaporation, Cd in the flue gas migrates downstream from the boiler chamber to the stack, where it undergoes condensation onto PFA particulates and DG due to a decrease in temperature within electrostatic precipitators and desulfurization unit (Appendix A Fig. S2). Despite the similarity in Cd isotope composition between the FC and the evaporated phase according to our aforementioned deduction, a positive fractionation of Cd isotopes was observed between PFA or DG and FC ($\Delta^{114}Cd_{PFA\text{-}FC}$ = 0.304‰, $\Delta^{114}Cd_{DG\text{-}FC}$ = 0.269‰) (Fig. 2a). This suggests an enrichment of heavier Cd isotopes during the condensation processes. Fouskas et al. (2018) also observed similar processes at two coal-fired power plants in the United States, demonstrating that heavy Cd isotopes condense on the surface of PFA particles during cooling. However, not all evaporated Cd condenses onto PFA or DG and is captured; instead, a portion of it still escapes into the atmosphere along with minute particles (Nussbaumer, 2007). Our results indicate that the escaped Cd exhibits an enrichment in lighter isotopes (e.g., $PM_{2.5}$). Additionally, we observed a positive variability between the proportion of escaped larger particles and both δ^{114}Cd values and Cd concentrations among particulate matter (TSP, PM_{10}, and $PM_{2.5}$), as depicted in Fig. 2a. These findings highlight the significant influence of particle size on both Cd isotopic fractionation and distribution.

Considering the positive correlation observed between Cd and Pb concentrations in both FC and combustion products (Appendix A Fig. S3), we propose that the behavior of Cd discussed above is also applicable to Pb. The disparity in Pb isotope ratios among combustion products (Fig. 2b) may be attributed to the heterogeneous distribution of Pb within coal (Bi et al., 2017). Combustible substances constitute the predominant component of coal composition (~95%) (Meij and Winkel, 2007). During high-temperature combustion, these

combustible substances exhibiting higher $^{208}Pb/^{206}Pb$ values were volatilized and introduced into the flue gas. Meanwhile, Pb combined with non-combustible substances could continuously accumulate in BA, resulting in lower $^{208}Pb/^{206}Pb$ values. This is further supported by the similarity in Pb isotope ratios between FC and deposition (Fig. 2b). During the condensing process within electrostatic precipitators and desulfurization unit, volatiles containing a higher $^{208}Pb/^{206}Pb$ ratio were incorporated into PFA and DG, resulting in their Pb isotope ratios falling between those of BA and depositions (Fig. 2b).

Overall, our findings suggest a two-stage condensation process that independently governs the distribution and isotopic differentiation of Cd and Pb, with particle size highlighting its significant influence on their behaviors. Heavy Cd isotopes preferentially accumulate on PFA during the stack condensation process. Subsequently, upon release from the stack, lighter Cd isotopes further selectively condense onto fine particles in the atmosphere (e.g., $PM_{2.5}$).

3.2. *Evaluation of Cd and Pb diffusion*

3.2.1. *Spatial distribution of Cd and Pb in deposition*

The atmospheric deposition flux serves as an indicator of the quantities of Cd and Pb released from the power plant (Marticorena et al., 2017). The magnitudes of Cd and Pb fluxes exhibited significant differences, with Pb being higher than Cd. However, they still demonstrated robust coherence, with significantly higher values predominantly observed in the S, N, and E directions compared to other directions (Fig. 3a, b). This indicates that despite the varying emission levels of Cd and Pb from the power plant, the diffusion patterns are governed by common factors. A decrease in Cd and Pb fluxes was observed with increasing distance in the NW–W–SW directions, while an increase in fluxes was noted with distance in the NE direction, aligning consistently with prevailing wind patterns (Appendix A Fig. S1). This suggests that the influence of wind parameters on Cd and Pb distribution is significant, leading to the long-distance transportation of coarse particles that would otherwise settle near the power plant. Given that larger particles exhibit a heavier isotopic composition compared to their smaller counterparts, wind can efficiently transport substantial quantities of these coarse particulates over considerable distances, leading to a wide distribution of heavier Cd isotopes. This aligns with the observed distribution characteristics of Cd isotopes in atmospheric deposition (Fig. 3c), providing further evidence for the influence of wind on the diffusion of Cd and Pb from the power plant.

3.2.2. *Spatial distribution of Cd and Pb in top soil*

Atmospheric deposition serves as the primary mechanism for the transfer of Cd and Pb from power plants, with the surrounding soil a long-term sink for these heavy metals (Hu et al., 2021). The distribution of Cd and Pb in top soil exhibited a strong positive correlation (Fig. 3d, e); however, unlike the deposition distribution pattern, the distribution of Cd and Pb in the top soil did not always correlate with the dominant wind circulation. This pattern of uncorrelated prevailing winds was also observed in the soil surrounding power plants located in Candiota, Brazil (da Silva Júnior et al., 2019) and Novocherkassk, Russia (Linnik et al., 2019). Within the scope of our investigation, elevated levels of Cd and Pb were observed in downwind directions (except for the N direction), indicating the influence of wind-driven diffusion and accumulation of these metals in the soil (Fig. 3d, e). In the N direction, an increase in soil concentrations of Cd and Pb was observed with distance, likely attributed to long-range dispersion of atmospheric heavy metals by wind beyond the scope of our study. Additionally, elevated levels of Cd and Pb were also observed in the S–SW directions, with a slight decrease as distance increased along these directions (Fig. 3d, e). This spatial accumulation of heavy metals in upwind directions may be attributed to the long-term deposition and subsequent leaching or wind dispersion of BA, PFA, and DG on-site into the surrounding soil (Wang et al., 2016). Overall, the accumulation of Cd and Pb in soil around the power plant has been demonstrated to be influenced not only by wind, but also by the secondary migration of these metals.

3.3. *Source tracing of Cd and Pb*

3.3.1. *Deposition*

In addition to site #S2 with an unusually high Pb concentration, there is a strong positive correlation between the Cd and Pb concentrations in the remaining atmospheric depositions (Appendix A Fig. S4), suggesting that these two heavy metals in the depositions likely have similar sources. Limited information is available regarding Cd isotopes in deposition; however, we have observed a significant disparity in Cd isotope compositions among depositions from different sampling sites. Generally, Cd isotopes tend to be heavier in the S–W–NW and NE directions, while $\delta^{114}Cd$ values decrease with increasing distance in the E–SE directions (Fig. 3c). The Cd isotope composition of most depositions exhibited a similarity to that observed in combustion emissions from the power plant, thereby indicating a direct contribution of the power plant. For example, the captured byproducts (BA, PFA, and DG), which are stored in exposed areas surrounding the power plant, may be dispersed into the atmosphere by wind currents (Schneider et al., 2021; Sherman et al., 2012). However, certain deposition samples exhibited significantly lighter Cd isotopic signatures that were outside the range observed in byproducts, such as #SE3 and #E3 (Fig. 2a). Based on our previous discussion, the emission of Cd isotopes in flue gas from the stack shows a decreasing trend with decreasing particle size. The depositions with the lightest Cd isotopic composition may contain materials consisting of particles smaller than 2.5 μm. Additionally, these sites may be influenced by other anthropogenic activities, such as traffic activity, which have relatively lighter Cd isotopic compositions ranging from –0.40‰ to –0.13‰ (Fang et al., 2022; Yan et al., 2021b; Zhang et al., 2020). Therefore, related transportation activities, such as the transportation of FC and combustion residues, can produce road dust and exhaust emissions as a source of metals in atmospheric deposition. This is further supported by the Pb isotope ratios observed in road dust (Duzgoren-Aydin, 2007) and automobile exhaust (Wang et al., 2021b) (Fig. 4). In general, in addition to direct emissions from the power plant stack, the long-term dispersal of BA, PFA, and DG by wind and large-scale industrial transport associated with the power plant constitutes significant sources of deposition.

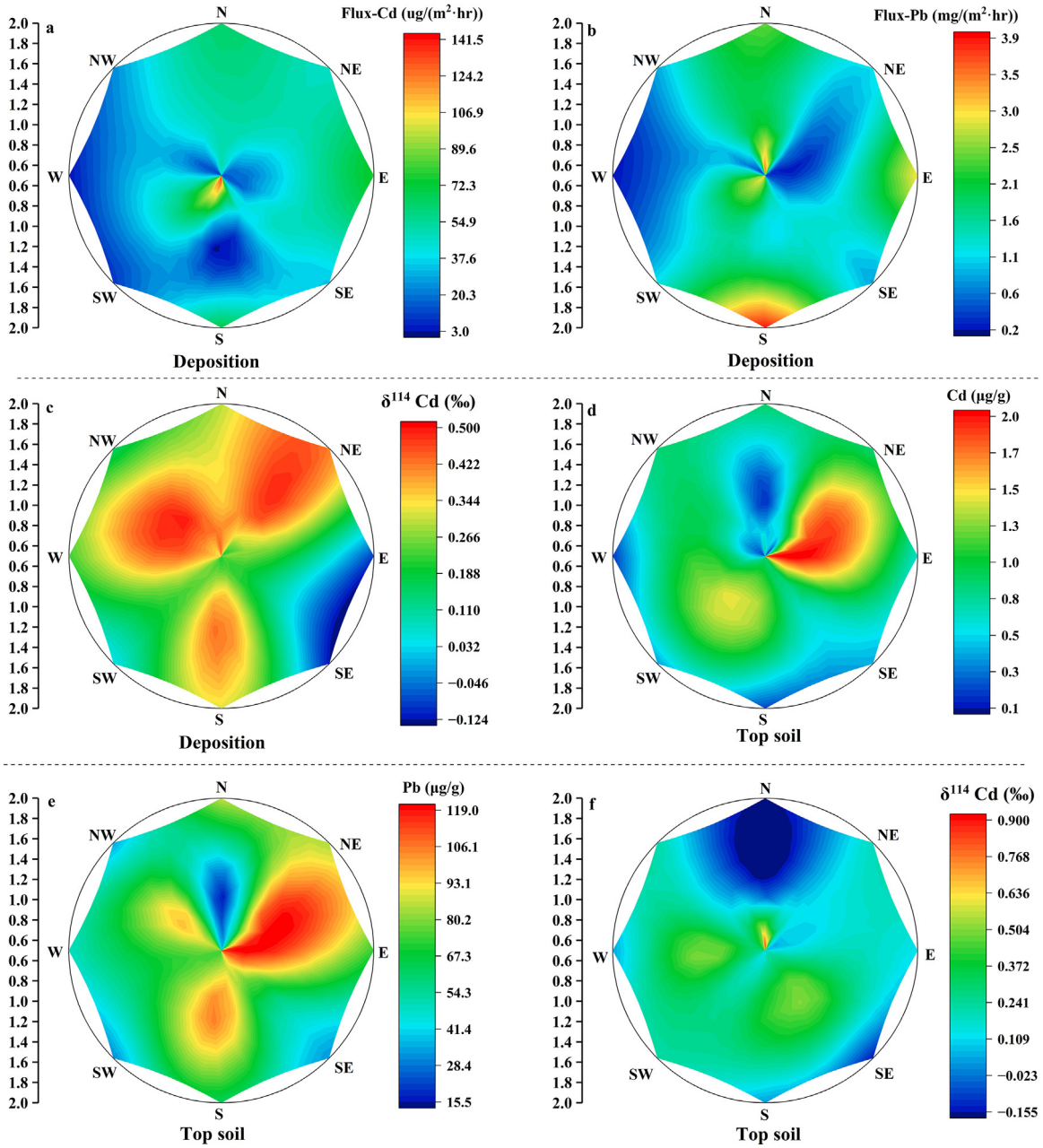

Fig. 3 – The sedimentation flux distribution of Cd (a) and Pb (b) in deposition, the Cd isotope composition distribution of deposition (c), the concentration distribution of top soil in Cd (d) and Pb (e), and the Cd isotope composition distribution of top soils (f).

3.3.2. *Top soil*

The concentrations of Cd in 95.5% and Pb in 81.8% of the soil samples are higher than those in bedrock (0.11 μg/g for Cd and 50.9 μg/g for Pb) (Liu et al., 2022), indicating that a majority of the Cd and Pb present in the soil originates from external sources. A positive correlation is also observed between the concentrations of Cd and Pb in top soils (Appendix A Fig. S5), suggesting a common source for these two heavy metals. Considering the Cd isotopic fractionation resulting from post-sedimentation processes (see Section 3.4), the Cd isotope signal originating from the power plant might be partially obscured, thereby exacerbating the challenge of source identification (Chrastný et al., 2015; Imseng et al., 2018). The absence of similar distribution characteristics of Cd concentrations and Cd isotopes in the soil further reinforces this understanding (Fig. 3f). Therefore, we used $^{206}Pb/^{207}Pb$ vs. $^{208}Pb/^{206}Pb$ to constrain the source of both Pb and Cd in top soils. As shown in Fig. 4, the Pb isotope compositions of top soil can be well fitted using a binary mixing model combining depositions and bottom soils from the profile as end-members. Thereupon, we employed the Bayesian model to quantitatively assess the relative contributions of deposition (as a power plant source) and bottom soils (as a natural source) to Cd and Pb in top soil. The results demonstrated a decline in the impact

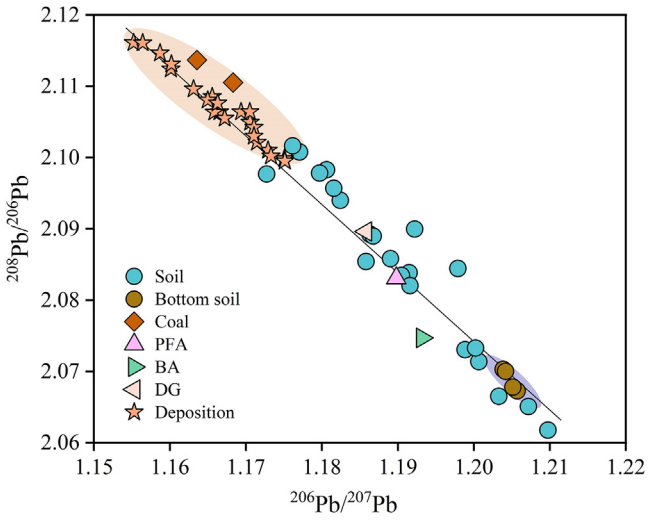

Fig. 4 – Diagram of $^{206}Pb/^{207}Pb$ versus $^{208}Pb/^{206}Pb$ for source tracing.

of the power plant as distance increased in the E, S, SE, SW, and W directions (Fig. 5). The influence accounted for 47%–80% when situated at a distance of 0.5 km, which subsequently decreased to below 10% (except #E3 to 34%) at a distance of 2 km (Appendix A Table S2). In contrast, power plant exhibited remarkably high contributions to soil pollution in the NW–N–NE directions, even at far distances (69%, 66%, and 79%). This observation suggests wind-assisted dispersion of emitted materials from the power plant over a distance that exceeds 2 km (Fig. 5). These observations substantiated the pervasive impact of the power plant on distant regions (Habib and Khan, 2021; Koffman et al., 2022; Mukai et al., 1993).

3.4. *Vertical behavior of historically deposited Cd and Pb in soils*

Our data showed that Cd and Pb primarily accumulate within the top 30 cm of the soil profile and move closer to the natural background as the depth increases (Appendix A Fig. S6), which is consistent with the findings of Wang et al. (2016). This suggests that despite the implementation of advanced emission control technologies at the power plant, historical emissions of Cd and Pb have persistently impacted the top 30 cm of soil over a prolonged period, posing a substantial threat to the surrounding environment and human health (Henneman et al., 2023; Minichilli et al., 2019). However, the Cd isotope composition of the top 30 cm of soil cannot be adequately explained by a single mixing relationship between deposition and bottom soil. For example, the Cd isotope composition of the 20–30 cm horizon (0.677‰ ± 0.051‰) is comparatively heavier than that of both deposition and bottom soil, implying potential post-depositional processes influencing historically deposited Cd in soils. Previous studies have demonstrated a preferential release of heavier Cd isotopes into solution, while lighter Cd isotopes exhibit a tendency to be retained in solid phases during the leaching process (Imseng et al., 2018; Zhang et al., 2016). This elucidates the potential transformation of heavy Cd isotopes into the subsurface stratum, resulting in an enrichment of heavy Cd isotopes in the 30 cm horizon. The Cd isotope composition (0.121‰ ± 0.033‰) of the uppermost soil layer in the profile exhibits a lighter value compared to that of the corresponding deposition ($\delta^{114}Cd = 0.450‰ \pm 0.060‰$ at site #NE2), providing further support for this conclusion.

Given that Pb isotope ratios remain undifferentiated during migration within the soil profile, if leaching occurs in a manner similar to Cd, the Pb isotope ratios of soils in the upper 30 cm should exhibit consistency. However, we observed a distinct disparity in Pb isotope ratios between the 0–10 cm and 10–30 cm soil layers (Appendix A Fig. S6), indicating negligible or minimal downward percolation of Pb. Furthermore, the ash generated by power plants exhibits a predominant enrichment of Cd in the re-release component, whereas Pb primarily remains in a residual fraction (Zhang et al., 2017; Zhao et al., 2018), providing further evidence that Cd is more prone to downward transfer through leaching. Therefore, the observed disparities in Pb isotope ratios among soils within the upper 30 cm may indicate significant temporal variations

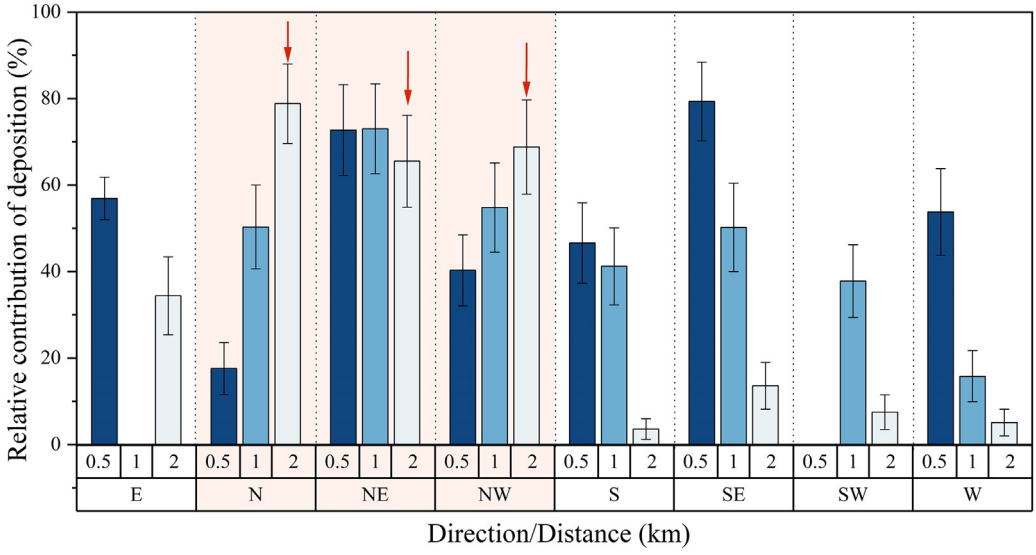

Fig. 5 – Contributions of deposition to top soil pollution.

in emissions over the six-decade operational history of the coal-fired power plant. This could be linked to advancements in pollution control technology and the implementation of environmentally friendly discharge treatment practices over the past two decades (Li et al., 2021; Peng et al., 2020; Wang et al., 2020). As discussed in Section 3.1, the combustion products in the two-stage condensation process of the power plant exhibited distinct Pb isotopic ratios. The PFA and DG captured during the first stage of condensation displayed relatively low $^{208}Pb/^{206}Pb$ values, which closely resemble those observed in the soil at a depth of 10–30 cm within the profile (Appendix A Fig. S6). This implies that in cases when dust removal technology is insufficient and operational efficiency is low, a substantial quantity of uncollected PFA from the power plant will be directly released into the surrounding soil (Wang et al., 2020). In contrast, the soil from 0–10 cm exhibited higher $^{208}Pb/^{206}Pb$ values similar to atmospheric deposition, indicating efficient capture of most condensed Pb within electrostatic precipitators and desulfurization unit, but releasing the Pb that had condensed in the second stage and was discharged from the stack. Therefore, the soils surrounding the power plant function as natural repositories, where soil materials intermingle with anthropogenic byproducts. The vertical variation in soil Pb reflects the historical evolution of human activities, thus rendering the adjacent soil a testament to the developmental history of the power plant.

4. Conclusions

The coal combustion products from a coal-fired power plant in southern China, as well as deposition and top soil were subjected to concentration and isotope analysis of Cd and Pb in this study. By combining Cd and Pb isotope ratios, a more comprehensive understanding of the behavior and distribution of Cd and Pb can be achieved, shedding light on the pollution effects exerted by the power plant on its surrounding soil. The main findings are as follows: (1) A two-stage condensation process governs the behavior of Cd and Pb during coal combustion, wherein particle size plays a crucial role. (2) The diffusion of Cd and Pb in deposition is mainly influenced by prevailing wind, while the distribution of these metals in soil is not solely controlled by wind but also potentially impacted by re-migration of long-term stored byproducts. (3) The long-term dispersion of byproducts and large-scale transport, in addition to emissions directly released from the stack, significantly constitute to deposition. The power plant significantly contributes to soil pollution in the NW–N–NE directions, even at a considerable distance, indicating its widespread influence on remote regions along these orientations. (4) Cd exhibits a propensity for downward migration through leaching within the soil profile, while variations in Pb respond to the historical progression of dust removal.

Declaration of Competing Interest

The authors declare that they have no known competing financial interests or personal relationships that could have appeared to influence the work reported in this paper.

Acknowledgments

This work was supported by the National Natural Science Foundation of China (No. 42025705), the Construction Project of Modern Agricultural Science and Technology Innovation Alliance of Guangdong Province, China (No. 2023KJ112), the National Natural Science Foundation of China (Nos. 41977291 and 42177242), and the GDAS'Project of Science and Technology Development, China (No. 2019GDASYL-0103048). We thank Dr. Yang Tang, Dr. Hui Chang, and Dr. Zhuo Lu for their invaluable assistance with isotope measurements.

Appendix A Supplementary data

Supplementary material associated with this article can be found in the online version at doi:10.1016/j.jes.2024.03.002.

References

Bi, X.Y., Li, Z.G., Wang, S.X., Zhang, L., Xu, R., Liu, J.L., et al., 2017. Lead isotopic compositions of selected coals, Pb/Zn ores and fuels in China and the application for source tracing. Environ. Sci. Technol. 51, 13502–13508.

Chang, H., Zhu, J.M., Wang, X.L., Gao, T., 2023. High-precision measurement of Cd isotopes in ultra-trace Cd samples using double spike-standard addition MC-ICP-MS. J. Anal. At. Spectrom. 38, 950–962.

Chrastný, V., Čadková, E., Vaněk, A., Teper, L., Cabala, J., Komárek, M., 2015. Cadmium isotope fractionation within the soil profile complicates source identification in relation to Pb–Zn mining and smelting processes. Chem. Geol. 405, 1–9.

Cloquet, C., Carignan, J., Libourel, G., Sterckeman, T., Perdrix, E., 2006. Tracing source pollution in soils using cadmium and lead isotopes. Environ. Sci. Technol. 40, 2525–2530.

da Silva Júnior, F.M.R., Ramires, P.F., dos Santos, M., Seus, E.R., Soares, M.C.F., Muccillo-Baisch, A.L., et al., 2019. Distribution of potentially harmful elements in soils around a large coal-fired power plant. Environ. Geochem. Health 41, 2131–2143.

Duzgoren-Aydin, N.S., 2007. Sources and characteristics of lead pollution in the urban environment of Guangzhou. Sci. Total Environ. 385, 182–195.

Fang, T., Wang, H., Liang, Y., Cui, K., Yang, K., Lu, W., et al., 2022. Source tracing with cadmium isotope and risk assessment of heavy metals in sediment of an urban river, China. Environ. Pollut. 305, 119325.

Fouskas, F., Ma, L., Engle, M.A., Ruppert, L., Geboy, N.J., Costa, M.A., 2018. Cadmium isotope fractionation during coal combustion: insights from two U.S. coal-fired power plants. Appl. Geochem. 96, 100–112.

Franssens, M., Flament, P., Deboudt, K., Weis, D., Perdrix, E., 2004. Evidencing lead deposition at the urban scale using "short-lived" isotopic signatures of the source term (Pb–Zn refinery). Atmos. Environ. 38, 5157–5168.

Habib, M.A., Khan, R., 2021. Environmental impacts of coal-mining and coal-fired power-plant activities in a developing country with global context. In: Shit, P.K., Adhikary, P.P., Sengupta, D. (Eds.), Spatial Modeling and Assessment of Environmental Contaminants: Risk Assessment and Remediation. Springer International Publishing, Cham, pp. 421–493.

He, B., Zhao, X., Li, P., Liang, J., Fan, Q., Ma, X., et al., 2019. Lead isotopic fingerprinting as a tracer to identify the pollution sources of heavy metals in the southeastern zone of Baiyin, China. Sci. Total Environ. 660, 348–357.

Henneman, L.R., Rasel, M.M., Choirat, C., Anenberg, S.C., Zigler, C., 2023. Inequitable exposures to US coal power plant–related $PM_{2.5}$: 22 years and counting. Environ. Health Perspect. 131, 037005.

Hu, Y.H., You, M., Liu, G.J., Dong, Z.B., 2021. Characteristics and potential ecological risks of heavy metal pollution in surface soil around coal-fired power plant. Environ. Earth Sci. 80 (17), 566.

Imseng, M., Wiggenhauser, M., Keller, A., Muller, M., Rehkamper, M., Murphy, K., et al., 2018. Fate of Cd in agricultural soils: a stable isotope approach to anthropogenic impact, soil formation, and soil-plant cycling. Environ. Sci. Technol. 52, 1919–1928.

Koffman, B.G., Saylor, P., Zhong, R., Sethares, L., Yoder, M.F., Hanschka, L., et al., 2022. Provenance of anthropogenic Pb and atmospheric dust to Northwestern North America. Environ. Sci. Technol. 56, 13107–13118.

Li, J., Zhuang, X.G., Querol, X., Font, O., Moreno, N., 2018. A review on the applications of coal combustion products in China. Int. Geol. Rev. 60, 671–716.

Kotelnikova, A.D., Rogova, O.B., Karpukhina, E.A., Solopov, A.B., Levin, I.S., Levkina, V.V., et al., 2022. Assessment of the structure, composition, and agrochemical properties of fly ash and ash-and-slug waste from coal-fired power plants for their possible use as soil ameliorants. J. Clean. Prod. 333, 130088.

Li, P., Lin, Z., Du, H., Feng, T., Zuo, J., 2021. Do environmental taxes reduce air pollution? Evidence from fossil-fuel power plants in China. J. Environ. Manage. 295, 113112.

Linnik, V.G., Minkina, T.M., Bauer, T.V., Saveliev, A.A., Mandzhieva, S.S., 2019. Geochemical assessment and spatial analysis of heavy metals pollution around coal-fired power station. Environ. Geochem. Health 42, 4087–4100.

Liu, Y., Xia, Y., Wang, Z., Gao, T., Zhu, J.M., Qi, M., et al., 2022. Lithologic controls on the mobility of Cd in mining-impacted watersheds revealed by stable Cd isotopes. Water Res. 220, 118619.

Lu, Z., Zhu, J.-M., Tan, D., Johnson, T.M., Wang, X., 2023. Double spike-standard addition technique and its application in measuring isotopes. Anal. Chem. 95, 2253–2259.

Mandal, A., Sengupta, D., 2006. An assessment of soil contamination due to heavy metals around a coal-fired thermal power plant in India. Environ. Int. 51, 409–420.

Marticorena, B., Chatenet, B., Rajot, J.L., Bergametti, G., Deroubaix, A., Vincent, J., et al., 2017. Mineral dust over west and central Sahel: Seasonal patterns of dry and wet deposition fluxes from a pluriannual sampling (2006-2012). J. Geophys. Res. 122, 1338–1364.

Meij, R., Winkel, H.T., 2007. The emissions of heavy metals and persistent organic pollutants from modern coal-fired power stations. Atmos. Environ. 41, 9262–9272.

Minichilli, F., Gorini, F., Bustaffa, E., Cori, L., Bianchi, F., 2019. Mortality and hospitalization associated to emissions of a coal power plant: a population-based cohort study. Sci. Total Environ. 694, 133757.

Moore, J.W., Semmens, B.X., 2008. Incorporating uncertainty and prior information into stable isotope mixing models. Ecol. Lett. 11, 470–480.

Mukai, H., Furuta, N., Fujii, T., Ambe, Y., Sakamoto, K., Hashimoto, Y., 1993. Characterization of sources of lead in the urban air of Asia using ratios of stable lead isotopes. Environ. Sci. Technol. 27, 1347–1356.

Nussbaumer, T., 2007. Techno-economic assessment of particle removal in automatic wood combustion plants from 100 kW to 2 MW. In: 15th European Biomass Conference. International Conference Centre, Berlin, pp. 7–11.

Park, J., Son, Y., Noh, S., Bong, T., 2018. An evaluation of the environmental safety and geochemical characteristics of coal combustion products. KSCE J. Civ. Eng. 22, 1700–1708.

Peng, W., Dai, H.C., Guo, H., Purohit, P., Urpelainen, J., Wagner, F., et al., 2020. The critical role of policy enforcement in achieving health, air quality, and climate benefits from India's clean electricity transition. Environ. Sci. Technol. 54, 11720–11731.

Raj, D., Maiti, S.K., 2020. Risk assessment of potentially toxic elements in soils and vegetables around coal-fired thermal power plant: a case study of Dhanbad, India. Environ. Monit. Assess. 192, 699.

Schneider, L., Maher, W., Potts, J., Gruber, B., Batley, G., Taylor, A., et al., 2014. Recent history of sediment metal contamination in Lake Macquarie, Australia, and an assessment of ash handling procedure effectiveness in mitigating metal contamination from coal-fired power stations. Sci. Total Environ. 490, 659–670.

Schneider, L., Rose, N.L., Myllyvirta, L., Haberle, S., Lintern, A., Yuan, J., et al., 2021. Mercury atmospheric emission, deposition and isotopic fingerprinting from major coal-fired power plants in Australia: insights from palaeo-environmental analysis from sediment cores. Environ. Pollut. 287, 117596.

Sherman, L.S., Blum, J.D., Keeler, G.J., Demers, J.D., Dvonch, J.T., 2012. Investigation of local mercury deposition from a coal-fired power plant using mercury isotopes. Environ. Sci. Technol. 46, 382–390.

Tan, D.C., Zhu, J.M., Wang, X.L., Han, G.L., Lu, Z., Xu, W.P., 2020. High-sensitivity determination of Cd isotopes in low-Cd geological samples by double spike MC-ICP-MS. J. Anal. At. Spectrom. 35, 713–727.

Tanić, M.N., Ćujić, M.R., Gajić, B.A., Daković, M.Z., Dragović, S.D., 2018. Content of the potentially harmful elements in soil around the major coal-fired power plant in Serbia: relation to soil characteristics, evaluation of spatial distribution and source apportionment. Environ. Earth Sci. 77 (1), 28.

Tong, Y.L., Gao, J.J., Ma, J.Y., 2023a. Emission characteristics, speciation, and potential environmental risks of heavy metals from coal-fired boilers: a review. Sustainability 15 (15), 11653.

Tong, Y.L., Gao, J.J., Yue, T., Zhang, X.X., Liu, J.Y., Bai, J., 2023b. Distribution, chemical fractionation, and potential environmental risks of Hg, Cr, Cd, Pb, and As in wastes from ultra-low emission coal-fired industrial boilers in China. J. Hazard. Mater. 446, 130606.

Tsikritzis, L.I., Ganatsios, S.S., Duliu, O.G., Kavouridis, C.V., Sawidis, T.D., 2002. Trace elements distribution in soil in areas of lignite power plants of western macedonia. J. Trace Microprobe Tech. 20, 269–282.

Vardar, S., Demirel, B., Onay, T.T., 2022. Impacts of coal-fired power plants for energy generation on environment and future implications of energy policy for Turkey. Environ. Sci. Pollut. Res. 29, 40302–40318.

Wang, G., Deng, J., Zhang, Y., Zhang, Q., Duan, L., Hao, J., et al., 2020. Air pollutant emissions from coal-fired power plants in China over the past two decades. Sci. Total Environ. 741, 140326.

Wang, H., Zhang, P., 2021. Emission characteristics of PM, heavy metals, and dioxins in flue gases from sintering machines with wet and semi-dry flue gas desulfurization systems. Environ. Sci. Pollut. Res. 28, 46089–46099.

Wang, L., Jin, Y., Weiss, D.J., Schleicher, N.J., Wilcke, W., Wu, L., et al., 2021a. Possible application of stable isotope compositions for the identification of metal sources in soil. J. Hazard. Mater. 407, 124812.

Wang, X., Zeng, X., Liu, C., Li, F., Xu, X., Lv, Y., 2016. Heavy metal contaminations in soil-rice system: source identification in relation to a sulfur-rich coal burning power plant in Northern Guangdong Province, China. Environ. Monit. Assess. 188, 460.

Wang, Y., Guo, G., Zhang, D., Lei, M., 2021b. An integrated method for source apportionment of heavy metal(loid)s in agricultural soils and model uncertainty analysis. Environ. Pollut. 276, 116666.

Wang, Z., Dai, S., Cowan, E.A., Dietrich, M., Schlesinger, W.H., Wu, Q., et al., 2023. Isotopic signatures and outputs of lead from coal fly ash disposal in China, India, and the United States. Environ. Sci. Technol. 57, 12259–12269.
Wiederhold, J.G., 2015. Metal stable isotope signatures as tracers in environmental geochemistry. Environ. Sci. Technol. 49, 2606–2624.
Wiggenhauser, M., Aucour, A.-M., Bureau, S., Campillo, S., Telouk, P., Romani, M., et al., 2021. Cadmium transfer in contaminated soil-rice systems: Insights from solid-state speciation analysis and stable isotope fractionation. Environ. Pollut. 269, 115934.
Xia, Y.F., Liu, Y.H., Liu, C.S., Gao, T., Yin, R.S., Qi, M., et al., 2023. Lake sediment archive reveals a distinct response to anthropogenic Pb and Zn deposition with historical periods: Pb-Zn isotope evidence. Environ. Sci. Technol. 57, 15184–15192.
Xie, X., Luo, J., Guan, L., Zhong, W., Jing, C., Wang, Y., 2021. Cadmium isotope fractionation during leaching with nitrilotriacetic acid. Chem. Geol. 584, 120523.
Yan, X.R., Zhu, M.Q., Li, W., Peacock, C.L., Ma, J.Y., Wen, H.J., et al., 2021a. Cadmium isotope fractionation during adsorption and substitution with iron (oxyhydr)oxides. Environ. Sci. Technol. 55, 11601–11611.
Yan, Y., Sun, Q., Yang, J., Zhang, X., Guo, B., 2021b. Source attributions of Cadmium contamination in rice grains by Cadmium isotope composition analysis: a field study. Ecotoxicol. Environ. Saf. 210, 111865.
Zhang, X.W., Yan, Y., Wadood, S.A., Sun, Q.Q., Guo, B.L., 2020. Source apportionment of cadmium pollution in agricultural soil based on cadmium isotope ratio analysis. Appl. Geochem. 123, 104776.
Zhang, Y., Shang, P., Wang, J., Norris, P., Romero, C.E., Pan, W.-p., 2017. Trace element (Hg, As, Cr, Cd, Pb) distribution and speciation in coal-fired power plants. Fuel 208, 647–654.
Zhang, Y., Wen, H., Zhu, C., Fan, H., Luo, C., Liu, J., et al., 2016. Cd isotope fractionation during simulated and natural weathering. Environ. Pollut. 216, 9–17.
Zhao, S., Duan, Y., Lu, J., Gupta, R., Pudasainee, D., Liu, S., et al., 2018. Chemical speciation and leaching characteristics of hazardous trace elements in coal and fly ash from coal-fired power plants. Fuel 232, 463–469.
Zhao, Y., Li, Y., Wiggenhauser, M., Yang, J., Sarret, G., Cheng, Q., et al., 2021. Theoretical isotope fractionation of cadmium during complexation with organic ligands. Chem. Geol. 571, 120178.
Zhao, Z.-Q., Zhang, W., Li, X.-D., Yang, Z., Zheng, H.-Y., Ding, H., et al., 2015. Atmospheric lead in urban Guiyang, Southwest China: isotopic source signatures. Atmos. Environ. 115, 163–169.
Zhong, Q., Zhou, Y., Tsang, D.C.W., Liu, J., Yang, X., Yin, M., et al., 2020. Cadmium isotopes as tracers in environmental studies: a review. Sci. Total Environ. 736, 139585.
Zhu, X.K., Guo, Y., Williams, R.J.P., O'Nions, R.K., Matthews, A., Belshaw, N.S., et al., 2002. Mass fractionation processes of transition metal isotopes. Earth Planet. Sci. Lett. 200, 47–62.